Peiman Naseradinmousavi
Assistant Professor
Dynamic Systems and Control Laboratory,
Department of Mechanical Engineering,
San Diego State University,
San Diego, CA 92115
e-mails: pnaseradinmousavi@mail.sdsu.edu;
peiman.n.mousavi@gmail.com

David B. Segala
Naval Undersea Warfare Center,
1176 Howell Street,
Newport, RI 02841
e-mail: david.segala@navy.mil

C. Nataraj
Mr. & Mrs. Robert F. Moritz
Senior Endowed Chair
Professor in Engineered Systems
The Villanova Center for Analytics of Dynamic Systems (VCADS),
Villanova University,
Villanova, PA 19085
e-mail: nataraj@villanova.edu

Chaotic and Hyperchaotic Dynamics of Smart Valves System Subject to a Sudden Contraction

In this paper, we focus on determining the safe operational domain of a coupled actuator–valve configuration. The so-called "smart valves" system has increasingly been used in critical applications and missions including municipal piping networks, oil and gas fields, petrochemical plants, and more importantly, the U.S. Navy ships. A comprehensive dynamic analysis is hence needed to be carried out for capturing dangerous behaviors observed repeatedly in practice. Using some powerful tools of nonlinear dynamic analysis including Lyapunov exponents and Poincaré map, a comprehensive stability map is provided in order to determine the safe operational domain of the network in addition to characterizing the responses obtained. Coupled chaotic and hyperchaotic dynamics of two coupled solenoid-actuated butterfly valves are captured by running the network for some critical values through interconnected flow loads affected by the coupled actuators' variables. The significant effect of an unstable configuration of the valve–actuator on another set is thoroughly investigated to discuss the expected stability issues of a remote set due to others and vice versa. [DOI: 10.1115/1.4033610]

1 Introduction

Multidisciplinary electromechanical–fluid systems have been widely used in many megascale networks. Municipal piping systems, oil and gas fields, petrochemical plants, and more critically, the U.S. Navy are the immediate ones which need to utilize a reliable, safe, and efficient coupled flow distribution network.

Future smart cities would inevitably need an autonomous flow control network in order to help improve the safety of such a critical system and also to decrease the incremental costs of operation and maintenance. Malfunctions of the flow network have occurred repeatedly resulting in the flow interruption of small towns/districts. Although significant cost and energy would be needed to be spent in order to restore the whole system in addition to human resources required to be recruited. Economical and even social impact of these malfunctions can be expected to be dramatic and consequently, a fully automated flow network is needed to be designed and operated.

The same issues exist for oil and gas fields and petrochemical plants. The industry of oil and gas is one of the most sensitive elements of the global economy and plays important roles even in global politics. The flow control network is the essential part of these fields and is therefore required to be safely designed to minimize the flow interruptions leading to much higher oil/gas production.

The U.S. National Defense and Homeland Security is undoubtedly a highly important priority which requires to be addressed and investigated carefully. The U.S. Navy broadly employs the network of coupled electromechanical valve sets for cooling purposes, mainly for chilled water systems. The proper performance of the network is remarkably effective for other critical units of radar, sonar, defense systems, etc.

We have carried out broad analytical and experimental studies from nonlinear modeling to design optimization of both an isolated and interconnected symmetric butterfly valves driven by solenoid actuators [1–8]. The multidisciplinary couplings, including electromagnetics and fluid mechanics, had to be thoroughly regarded in the modeling phase in order to yield an accurate nonlinear model of such a complex system. A third-order nondimensional dynamic model of the single set was derived to be used in nonlinear dynamic analysis [3] and optimal design [4].

The dynamic analysis expectedly yielded practically observed crisis and transient chaotic dynamics of a single actuated valve for some critical physical parameters. A comprehensive stability map was also presented as an efficient tool to determine the safe domain of operation which in turn could serve for identifying the lower and upper bounds of the design optimization efforts. The design optimization was then carried out [4] to select the optimal actuation unit's parameters coupled with the mechanical and fluid parts in order to significantly reduce the amount of energy consumption (upward of 40%).

Note that the applications addressed earlier contain thousands of actuated valves in which a high level of dynamic coupling has been repeatedly observed in practice. These dynamic couplings among different sets need to be captured through analytical studies. We have developed [5] a novel nonlinear model for two sets of solenoid-actuated butterfly valves operating in series. The closing/opening valves were modeled as changing resistors and the flow between them as a constant one. A sixth-order nonlinear coupled model revealed the high dynamic sensitivity of each element of a set, the valve and the actuator, to another one and vice versa. The power spectrum was used in confirming the same frequency response of a neighbor set due to the external periodic noise applied on another set of the valve and actuator.

In further studies, we optimized the design of coupled actuation units of two sets operating in series [8] subject to a sudden contraction. The pipe contraction imposed an additional resistance to be modeled, and therefore, the coupled dynamic equations derived in Ref. [5] had to be slightly modified. We represent the modeling process here for completeness. We have surprisingly established an interesting coupling between currents of the actuation units through the interconnected flow loads, including hydrodynamic and bearing torques, which affect both the valves' dynamics.

Important nonlinear phenomena in electromechanical systems have also received considerable attention. Sun et al. [9] studied

Contributed by the Design Engineering Division of ASME for publication in the Journal of Computational and Nonlinear Dynamics. Manuscript received March 9, 2016; final manuscript received April 29, 2016; published online June 2, 2016. Assoc. Editor: Stefano Lenci.

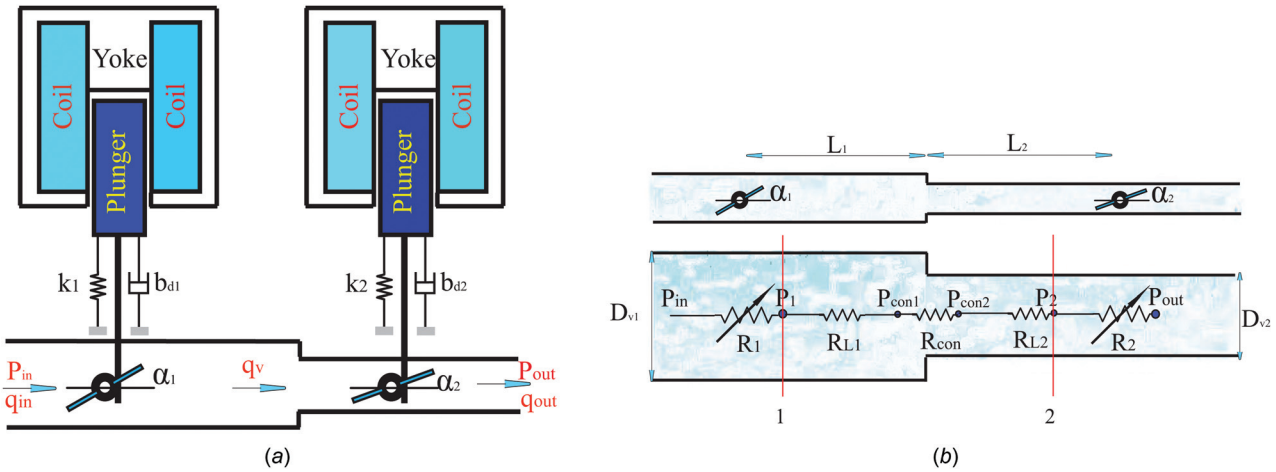

Fig. 1 (*a*) A schematic configuration of two solenoid-actuated butterfly valves subject to sudden contraction and (*b*) a coupled model of two butterfly valves in series without actuation

the hyperchaotic behavior of the newly presented simplified Lorenz system by using a sinusoidal parameter variation and hyperchaos control of the forced system via feedback. Banerjee et al. [10] investigated the synchronization of chaos and hyperchaos in first-order time-delayed systems that are coupled using the nonlinear time-delay excitatory coupling by assigning two characteristic time delays: the system delay that is same for both the systems and the coupling delay associated with the coupling path. Many efforts for analyzing hyperchaotic dynamics have been reported in Refs. [11–26].

We have addressed the modeling process subject to the pipe contraction in Ref. [8] and represent here for completeness. The contribution of this work is the inclusion of interconnected electromechanical–fluid nonlinearities between two actuator–valve configurations to thoroughly analyze the effects of an unstable set of the valve–actuator on another one. Through this comprehensive analysis, chaotic and hyperchaotic dynamics of two coupled configurations are captured by exposing the network to some critical values. The responses are then characterized using some powerful tools including Lyapunov exponents and Poincaré map.

2 Mathematical Modeling

Figure 1(*a*) shows a pair of symmetric butterfly valves driven by solenoid actuators through rack and pinion arrangements. The rack and pinion mechanism provides a kinematic constraint which connects the dynamics of the valve and actuator. Applying DC voltages, as being used in the Navy ships for chilled water systems, the motive forces give translational motions to the actuators' moving parts (plungers), and subsequently, the valves rotate to desirable angles. Note that a return spring has been a common practice among industries to open the valves.

Interconnected modeling of such a multiphysics system undoubtedly needs some simplifying assumptions to neglect useless and tremendously time-consuming numerical calculations. The magnetic force resulted from the magnetic field needs an extremely short period of time to reach its maximum value. This period is the so-called "diffusion time" and has an inverse relationship with the amount of current used. Note that using current of 4 A would yield a negligible diffusion time of $\tau_d \approx 20$ ms [1] with respect to the nominal operation time of 40 s. We have to also assume dominant laminar flow for both the coupled valves. Note that developing an analytical model is a necessity to carry out the dynamic analysis and optimization which would lead us to make such a commonly used assumption and also to avoid the numerical difficulties involved with a turbulent regime. However, a crucial question needs to be carefully answered with respect to the validity of such an assumption. Using the values of pipe diameter and flow mean velocity listed in Table 1, one can easily distinguish the existence of the turbulent regime which invalidates the assumption we have made. From another aspect, the analytical formulas derived for the flow loads, including the hydrodynamic and bearing torques, have been developed based on the assumption of laminar flow [27,28]. To address the issues discussed above, we have carried out experimental work to measure the sum of the hydrodynamic and bearing torques as the most affecting loads on the valves' and subsequently actuators' dynamics [8]. The experiment yielded the total torque (Fig. 2) for the inlet velocity of $v \approx 2.7$ m/s and valve diameter of $D_v = 2$ in. validating the laminar flow assumption [29]. The flow torques have shown highly important roles for the dynamics of an isolated solenoid-actuated butterfly valve and we hence expect to observe such effects for the interconnected sets [5].

The coupled system is modeled as a set of five resistors. Two changing resistors represent the closing/opening valves, two constant ones indicate head losses between the valves, and another is due to the pipe contraction as shown in Fig. 1(*b*). The inlet and outlet pressure values are given in Table 1. Using the assumption of the dominant laminar flow, the pressure drops between two valves can be expressed based on the Hagen–Poiseuille [30] and Borda–Carnot [31] formulas (points 1 and 2)

$$P_1 - P_{\text{con1}} = \underbrace{\frac{128\mu_f L_1}{\pi D_{v1}^4}}_{R_{L1}} q_v \tag{1}$$

$$P_{\text{con1}} - P_{\text{con2}} = \frac{1}{2} K_{\text{con}} \rho v_{\text{out}}^2 \tag{2}$$

Table 1 The system parameters

P	1000 kg/m^3	v	0.1 m/s
$J_{1,2}$	0.104×10^{-1} kg m^2	N_2	3000
N_1	3000	$C_{11,22}$	1.56×10^6 H^{-1}
$g_{m1,m2}$	0.1 m	$V_{1,2}$	24 V
D_{v1}	0.2032 m	D_{v2}	0.127 m
$D_{s1,s2}$	0.01 m	P_{out}	2 kPa
$k_{1,2}$	1000 N·m^{-1}	$C_{21,22}$	6.32×10^8 H^{-1}
L_1	2 m	L_2	1 m
μ_f	0.018 kg m^{-1} s^{-1}	$R_{1,2}$	6 Ω
$r_{1,2}$	0.05 m	θ	90 deg
P_{in}	256 kPa		

$$P_{con2} - P_2 = \underbrace{\frac{128\mu_f L_2}{\pi D_{v2}^4}}_{R_{L2}} q_v \tag{3}$$

where q_v is the volumetric flow rate, μ_f indicates the fluid dynamic viscosity, D_{v1} and D_{v2} are the valves' diameters, L_1 and L_2 stand for the pipe lengths before and after contraction, R_{L1} and R_{L2} indicate the constant resistances, and P_{con1} and P_{con2} are the flow pressures before and after contraction. K_{con} is calculated as follows:

$$K_{con} = 0.5\left(1 - \beta^2\right)\sqrt{\sin\left(\frac{\theta}{2}\right)} \tag{4}$$

where β indicates the ratio of minor and major diameters (D_{v2}/D_{v1}), and θ is the angle of approach. The values listed in Table 1 easily yield $K_{con} = 0.2562$. We then rewrite Eq. (2) as follows:

$$\begin{aligned} P_{con1} - P_{con2} &= \frac{1}{2}K_{con}\rho v_{out}^2 \\ &= \underbrace{\frac{8K_{con}}{\pi^2 D_{v2}^4}\rho}_{R_{con}} \underbrace{\frac{\pi^2 D_{v2}^4 v_{out}^2}{16}}_{q_v^2} \\ &= R_{con} q_v^2 \end{aligned} \tag{5}$$

where R_{con} is the resistance due to the pipe contraction. The pressure drop between the valves can be derived by adding Eqs. (1)–(3) and (5)

$$P_1 - P_2 = [R_{L1} + R_{L2} + R_{con} q_v] q_v \tag{6}$$

The valve's "resistance (R)" and "coefficient (c_v)," as important parameters of the regulating valves, are nonlinear functions of the valve rotation angle to be stated [32] as follows:

$$R_i(\alpha_i) = \frac{891 D_{vi}^4}{c_{vi}^2(\alpha_i)}, \quad i = 1, 2 \tag{7}$$

Based on the assumption of laminar flow, the valve's pressure drop is calculated via the following relationship [27]:

$$\Delta P_i(\alpha_i) = 0.5 R_i(\alpha_i)\rho v^2 \tag{8}$$

where α indicates the valve rotation angle, ρ is the density of the media, and v stands for the flow velocity. Rewriting Eq. (8) in the standard form gives

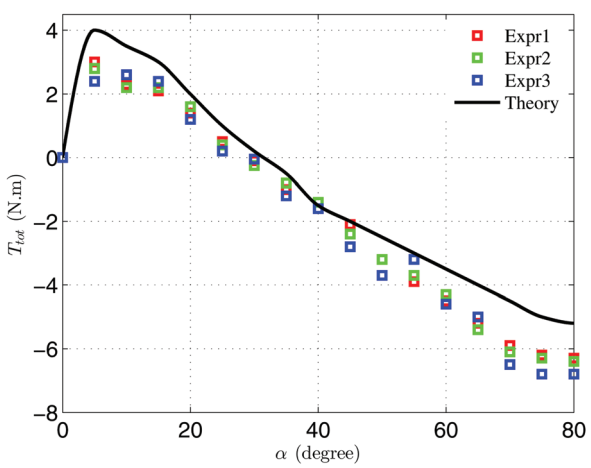

Fig. 2 A comparison between the experimental and analytical total torques

$$\Delta P_i(\alpha_i) = \underbrace{\frac{\pi^2 D_{vi}^4 v^2}{16}}_{q_v^2} \underbrace{\frac{8 \times R_i(\alpha_i)\rho}{\pi^2 D_{vi}^4}}_{R_{ni}(\alpha_i)} = R_{ni}(\alpha_i) q_v^2 \tag{9}$$

The hydrodynamic (T_h) and bearing (T_b) torques [27,28] have expectedly shown the high sensitivity to the pressure drop obtained via Eq. (9) leading us to rewrite them as follows:

$$f_i(\alpha_i) = \frac{16 T_{ci}(\alpha_i)}{3\pi\left(1 - \frac{C_{cci}(\alpha_i)\left(1 - \sin(\alpha_i)\right)}{2}\right)^2} \tag{10}$$

$$T_{hi} = \frac{16 T_{ci}(\alpha_i) D_{vi}^3 \Delta P_i}{3\pi\left(1 - \frac{C_{cci}(\alpha_i)\left(1 - \sin(\alpha_i)\right)}{2}\right)^2} = f_i(\alpha_i) D_{vi}^3 \Delta P_i \tag{11}$$

$$T_{bi} = 0.5 A_d \Delta P_i \mu D_s = C_i \Delta P_i \tag{12}$$

where D_s stands for the stem diameter of the valve, μ indicates the friction coefficient of the bearing area, $C_i = (\pi/8)\mu D_{vi}^2 D_s$, and T_{ci} and C_{cci} are the hydrodynamic torque and the sum of upper and lower contraction coefficients, respectively, depending on the valve rotation angle [1].

The comprehensive stability map we have presented in Ref. [3] was based on a nonlinear analytical model. The analytical model had to be used in the dynamic analysis to investigate the system stability around equilibria by calculating its eigenvalues through the Jacobian matrix; this has led us to identify the safe operational domain to be utilized in the design optimization. The same practice was employed in Ref. [8] with the aid of fitting suitable curves on c_{vi} and R_{ni} in order to model the system analytically. For our case study of $D_{v1} = 8$ in. and $D_{v2} = 5$ in., the valves' coefficients and resistances are developed as follows:

$$c_{v1}(\alpha_1) = p_1\alpha_1^3 + q_1\alpha_1^2 + o_1\alpha_1 + s_1 \tag{13}$$

$$c_{v2}(\alpha_2) = p_2\alpha_2^3 + q_2\alpha_2^2 + o_2\alpha_2 + s_2 \tag{14}$$

$$R_{n1}(\alpha_1) = \frac{e_1}{\left(p_1\alpha_1^3 + q_1\alpha_1^2 + o_1\alpha_1 + s_1\right)^2} \tag{15}$$

$$R_{n2}(\alpha_2) = \frac{e_2}{\left(p_2\alpha_2^3 + q_2\alpha_2^2 + o_2\alpha_2 + s_2\right)^2} \tag{16}$$

where $e_1 = 7.2 \times 10^5$, $p_1 = 461.9$, $q_1 = -405.4$, $o_1 = -1831$, $s_1 = 2207$, $e_2 = 4.51 \times 10^5$, $p_2 = 161.84$, $q_2 = -110.53$, $o_2 = -695.1$, and $s_2 = 807.57$. These fittings were selected with respect to the decremental and incremental profiles of the valves' coefficients and resistances, respectively [5,29]. Applying the mass continuity principle ($q_{in} = q_{out} = q_v$) and then rewriting Eq. (9) yield

$$\frac{P_{in} - P_1}{R_{n1}(\alpha_1)} = \frac{P_2 - P_{out}}{R_{n2}(\alpha_2)} \tag{17}$$

$$R_{n1}P_2 + R_{n2}P_1 = R_{n2}P_{in} + R_{n1}P_{out} \tag{18}$$

The interconnected P_1 and P_2 terms are derived by combining Eqs. (6) and (18) as follows:

$$P_1 = \frac{R_{n2}P_{in} + R_{n1}P_{out} + R_{n1}(R_{L1} + R_{L2} + R_{con}q_v)q_v}{(R_{n1} + R_{n2})} \tag{19}$$

$$P_2 = \frac{R_{n2}P_{in} + R_{n1}P_{out} - R_{n2}(R_{L1} + R_{L2} + R_{con}q_v)q_v}{(R_{n1} + R_{n2})} \tag{20}$$

The dynamic sensitivities of P_1 and P_2 to R_{n1}, R_{n2}, R_{L1}, R_{L2}, and R_{con} are distinguishable through Eqs. (19) and (20), as observed in the practice. Any slight dynamic changes of the upstream set of the valve–actuator would be expected to be observed for the downstream one. The hydrodynamic and bearing torques' dependencies on all the resistances are reformulated as follows:

$$T_{hi} = f_i(\alpha_i) D_{vi}^3 \Delta P_i(R_{n1}, R_{n2}, R_{L1}, R_{L2}, R_{\text{con}}) \tag{21}$$

$$T_{bi} = C_i \Delta P_i(R_{n1}, R_{n2}, R_{L1}, R_{L2}, R_{\text{con}}) \tag{22}$$

f_i is a nonlinear function of the changing T_{ci}, C_{cci}, and the valve rotation angle. To carry out a systematic dynamic analysis, the following functions are fitted to the $D_{vi}^3 f_i$ of each valve [5,29]:

$$\begin{aligned} T_{h1} &= \underbrace{\left(a_1\alpha_1 e^{b_1{\alpha_1}^{1.1}} - c_1 e^{d_1\alpha_1}\right)}_{D_{v1}^3 f_1}(P_{\text{in}} - P_1) \\ &= \left(a_1\alpha_1 e^{b_1{\alpha_1}^{1.1}} - c_1 e^{d_1\alpha_1}\right) \times \frac{e_1}{\left(p_1\alpha_1^3 + q_1\alpha_1^2 + o_1\alpha_1 + s_1\right)^2} \\ &\quad \times \sum_{i=1}^{2} \frac{e_i}{\left(p_i\alpha_i^3 + q_i\alpha_i^2 + o_i\alpha_i + s_i\right)^2} \\ &\quad \times (P_{\text{in}} - P_{\text{out}} - (R_{L1} + R_{L2} + R_{\text{con}} q_v) q_v) \end{aligned} \tag{23}$$

$$\begin{aligned} T_{h2} &= \underbrace{\left(a_1'\alpha_2 e^{b_1'{\alpha_2}^{1.1}} - c_1' e^{d_1'\alpha_2}\right)}_{D_{v2}^3 f_2}(P_2 - P_{\text{out}}) \\ &= \left(a_1'\alpha_2 e^{b_1'{\alpha_2}^{1.1}} - c_1' e^{d_1'\alpha_2}\right) \times \frac{e_2}{\left(p_2\alpha_2^3 + q_2\alpha_2^2 + o_2\alpha_2 + s_2\right)^2} \\ &\quad \times \sum_{i=1}^{2} \frac{e_i}{\left(p_i\alpha_i^3 + q_i\alpha_i^2 + o_i\alpha_i + s_i\right)^2} \\ &\quad \times (P_{\text{in}} - P_{\text{out}} - (R_{L1} + R_{L2} + R_{\text{con}} q_v) q_v) \end{aligned} \tag{24}$$

where $a_1 = 0.4249$, $a_1' = 0.1022$, $b_1 = -18.52$, $b_1' = -17.0795$, $c_1 = -7.823 \times 10^{-4}$, $c_1' = -2 \times 10^{-4}$, $d_1 = -1.084$, and $d_1' = -1.0973$.

We have previously derived the rate of current and magnetic force terms [1], which are utilized in developing the sixth-order coupled dynamic model [8] as follows. Note that both the motive force and current are highly sensitive to the plunger displacement and subsequently the valve rotation angle

$$F_{mi} = \frac{C_{2i} N_i^2 i_i^2}{2\left(C_{1i} + C_{2i}(g_{mi} - x_i)\right)^2} \tag{25}$$

$$\frac{di_i}{dt} = \frac{(V_i - R_i i_i)\left(C_{1i} + C_{2i}(g_{mi} - x_i)\right)}{N_i^2} - \frac{C_{2i} i_i \dot{x}_i}{\left(C_{1i} + C_{2i}(g_{mi} - x_i)\right)} \tag{26}$$

$$\dot{z}_1 = z_2 \tag{27}$$

$$\begin{aligned} \dot{z}_2 = \frac{1}{J_1}\Bigg[& \frac{r_1 C_{21} N_1^2 z_3^2}{2\left(C_{11} + C_{21}(g_{m1} - r_1 z_1)\right)^2} - b_{d1} z_2 - k_1 z_1 \\ & + \frac{(P_{\text{in}} - P_{\text{out}} - (R_{L1} + R_{L2} + R_{\text{con}} q_v) q_v) e_1}{\left(p_1 z_1^3 + q_1 z_1^2 + o_1 z_1 + s_1\right)^2} \\ & + \frac{}{\sum_{i=1,4} \frac{e_i}{\left(p_i z_i^3 + q_i z_i^2 + o_i z_i + s_i\right)^2}} \\ & \times \left[\left(a_1 z_1 e^{b_1{z_1}^{1.1}} - c_1 e^{d_1 z_1}\right) - C_1 \times \tanh(K z_2)\right]\Bigg] \end{aligned} \tag{28}$$

$$\dot{z}_3 = \frac{(V_1 - R_1 z_3)\left(C_{11} + C_{21}(g_{m1} - r_1 z_1)\right)}{N_1^2} - \frac{r_1 C_{21} z_3 z_2}{\left(C_{11} + C_{21}(g_{m1} - r_1 z_1)\right)} \tag{29}$$

$$\dot{z}_4 = z_5 \tag{30}$$

$$\begin{aligned} \dot{z}_5 = \frac{1}{J_2}\Bigg[& \frac{r_2 C_{22} N_2^2 z_6^2}{2\left(C_{12} + C_{22}(g_{m2} - r_2 z_4)\right)^2} - b_{d2} z_5 - k_2 z_4 \\ & + \frac{(P_{\text{in}} - P_{\text{out}} - (R_{L1} + R_{L2} + R_{\text{con}} q_v) q_v) e_2}{\left(p_2 z_4^3 + q_2 z_4^2 + o_2 z_4 + s_2\right)^2} \\ & + \frac{}{\sum_{i=1,4} \frac{e_i}{\left(p_i z_i^3 + q_i z_i^2 + o_i z_i + s_i\right)^2}} \\ & \times \left[\left(a_1' z_4 e^{b_1'{z_4}^{1.1}} - c_1' e^{d_1' z_4}\right) - C_2 \times \tanh(K z_5)\right]\Bigg] \end{aligned} \tag{31}$$

$$\dot{z}_6 = \frac{(V_2 - R_2 z_6)\left(C_{12} + C_{22}(g_{m2} - r_2 z_4)\right)}{N_2^2} - \frac{r_2 C_{22} z_5 z_6}{\left(C_{12} + C_{22}(g_{m2} - r_2 z_4)\right)} \tag{32}$$

where b_d indicates the equivalent torsional damping, K_t is the equivalent torsional stiffness, V stands for the supply voltage, x is the plunger displacement, r indicates the radius of the pinion, C_1 and C_2 are the reluctances of the magnetic path without air gap and that of the air gap, respectively, F_m is the motive force, N stands for the number of coils, i indicates the applied current, g_m is the nominal airgap, J indicates the polar moment of inertia of the valve's disk, and R is the electrical resistance of coil.

3 Linear Dynamic Analysis

The linearization method is one of the immediate tools to be used in determining the stability of the network around multiple equilibria. The analytical studies of such a six-state system would be tedious and time-consuming, in particular, in the presence of enormous parameters and variables. The numerical method is an optimal approach to calculate the Jacobian matrix shown in Eq. and subsequently the system's eigenvalues to judge the stability around the equilibria. We select two important critical parameters of the equivalent viscous damping (b_{di}) and the friction coefficient of bearing area (μ_i) of both the sets to evaluate their effects on the stability/instability of the coupled sets

$$J = \begin{bmatrix} 0 & 1 & 0 & 0 & 0 & 0 \\ 1732334 & j_{22} & 26 & -4772 & 0 & 0 \\ 0 & -1.95 & -43.17 & 0 & 0 & 0 \\ 0 & 0 & 0 & 0 & 1 & 0 \\ -1175.93 & 0 & 0 & 1957044 & j_{55} & 0 \\ 0 & 0 & 0 & -84.26 & 0 & -43.17 \end{bmatrix} \tag{33}$$

where $j_{22} = -96 b_{d1} - 177.13\mu_1$ and $j_{55} = -96.15 b_{d2} - 323.71\mu_2$.

We then obtain the following characteristic equation based on b_{di} and μ_i:

$$s^6 + Co_1 s^5 + Co_2 s^4 + Co_3 s^3 + Co_4 s^2 + Co_5 s + Co_6 = 0 \tag{34}$$

where

$$\text{Co}_1 = 96 b_{d1} + 96 b_{d2} + 177\mu_1 + 323\mu_2 + 86 \tag{35}$$

$$\begin{aligned} \text{Co}_2 = {} & 8302 b_{d1} + 8302 b_{d2} + 15295\mu_1 + 27951\mu_2 \\ & + 9245 b_{d1} b_{d2} + 31125 b_{d1}\mu_2 + 17032 b_{d2}\mu_1 \\ & + 57340\mu_1\mu_2 - 3687463 \end{aligned} \tag{36}$$

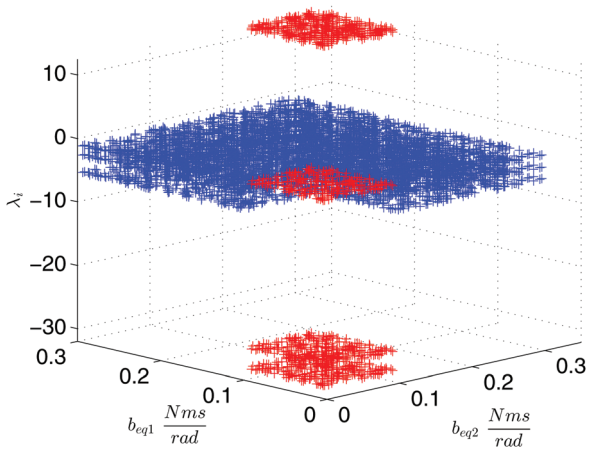

Fig. 3 The interconnected sets' stability map; $10^{-8} \le b_{di} = \mu_i \le 9\times10^{-2}$ and $10^{-1} \le b_{di} = \mu_i \le 3\times10^{-1}$ stand for unstable and stable domains, respectively

$$\begin{aligned} Co_3 = {} & 187998083b_{d1} + 166386463b_{d2} + 346333714\mu_1 \\ & + 560154376\mu_2 - 798323b_{d1}b_{d2} - 2687624b_{d1}\mu_2 \\ & - 1470686b_{d2}\mu_1 - 4951194\mu_1\mu_2 + 318563300 \end{aligned} \tag{37}$$

$$\begin{aligned} Co_4 = {} & -16248483272b_{d1} - 14382603305b_{d2} \\ & - 29933270986\mu_1 - 48420274134\mu_2 + 17233142b_{d1}b_{d2} \\ & + 58016860b_d\mu_2 + 31747229b_{d2}\mu_1 + 106879785\mu_1\mu_2 \\ & + 3383271986600 \end{aligned} \tag{38}$$

$$\begin{aligned} Co_5 = {} & 350750592245b_{d1} + 310477025305b_{d2} \\ & + 646159543021\mu_1 + 1045247675853\mu_2 \\ & - 292732345689222 \end{aligned} \tag{39}$$

$$Co_6 = 6319208419510455 \tag{40}$$

Using the numerical approach, the coupled sets' normalized eigenvalues are presented in Fig. 3 revealing an interesting stability map by assuming that b_{di}'s and μ_i's change equally for a critical range of $10^{-8} \le b_{di} = \mu_i \le 3 \times 10^{-1}$.

Figure 3 shows the instability and stability of the coupled sets for the ranges of $10^{-8} \le b_{di} = \mu_i \le 9 \times 10^{-2}$ and $10^{-1} \le b_{di} = \mu_i \le 3 \times 10^{-1}$ by presenting positive and negative real parts of eigenvalues, respectively. Such a stability map would help us select some critical values in order to capture practically observed chaotic and hyperchaotic dynamics.

4 Results

We select two sets of initial conditions for the critical values of $b_{di} = \mu_i = 10^{-7}$, based on the stability map shown in Fig. 3, as follows:

$$\text{Initial}_1 = [20(\text{deg})\,0\,0\,20(\text{deg})\,0\,0]$$

$$\text{Initial}_2 = [2(\text{deg})\,0\,0\,2(\text{deg})\,0\,0]$$

Chaotic motions are known to be sensitive to even slight changes of initial conditions and hence examining different initial conditions potentially serve to characterize the responses obtained. The first set, Initial_1, would be a realistic option for the so-called "modulating" valves to regulate/reroute flow for many applications addressed earlier. The second set, Initial_2, is chosen to be close enough to the system's physically feasible equilibrium point and also to avoid numerical singularities.

Figures 4(*a*) and 4(*b*) show the phase portraits of the coupled valves for two sets of the initial conditions. Figures 4(*a*) and 4(*b*) reveal coupled chaotic and hyperchaotic dynamics. The hyperchaotic attractors by having two or more positive lyapunov exponents [33] are also known to be sensitive to initial conditions, and subsequently, orbits initiated from two close points move expectedly away from each other until the separation reaches the size of attractor. Some power tools of the nonlinear dynamic analysis would potentially help us characterize the responses obtained, in particular, Lyapunov exponents and Poincaré maps shown in Figs. 5(*a*)–7(*b*). A chaotic attractor presents one positive Lyapunov exponent [33], as shown in Fig. 5(*a*) ($L_6 = +0.1535$), indicating the chaotic motions of the interconnected valves–actuators configuration. Figure 5(*b*) presents two positive Lyapunov exponents not only for the sudden pipe contraction ($\theta = 90$ deg) but also for a broad spectrum of the approach angles ($35\,\text{deg} \le \theta \le 85\,\text{deg}$), which can be served as a proof of the network's hyperchaotic dynamics. Poincaré map is another power tool to distinguish among periodic, quasi-periodic, and chaotic responses. Note that for an n-dimensional system ($n \ge 3$), this tool may not yield a clear nature of the response to determine whether the motion is chaotic or two-period quasi-periodic [33]. Although the Lyapunov exponents, as discussed earlier, would firmly confirm the chaotic and hyperchaotic motions of the interconnected actuated valves along with irregular Poincaré maps (almost different sets of 635 points) as shown in Figs. 6(*a*)–7(*b*) for each set of the upstream and downstream valves and for two sets of the initial conditions.

Figures 8(*a*) and 8(*b*) show the total flow loads, the sum of both the hydrodynamic and bearing torques versus the motive forces for two initial conditions. The squared areas remarkably magnify the differences between the chaotic and hyperchaotic responses of the coupled sets by presenting relatively larger attractor sizes for the hyperchaotic ones.

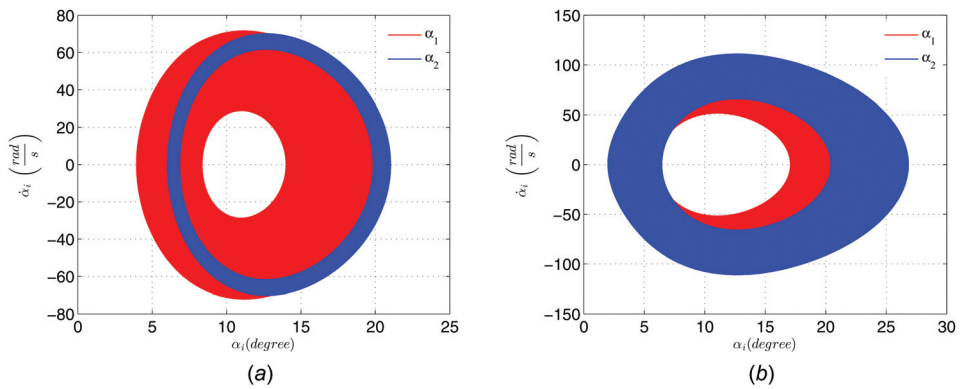

Fig. 4 (*a*) The coupled sets' phase portraits for Initial_1 and (*b*) the coupled sets' phase portraits for Initial_2

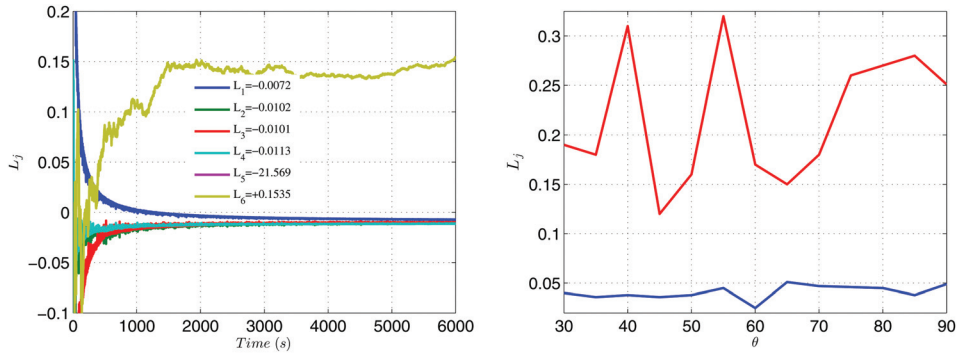

(*a*) (*b*)

Fig. 5 (*a*) The Lyapunov exponents for Initial$_1$ and (*b*) the positive Lyapunov exponents for Initial$_2$ versus different approach angles (θ)

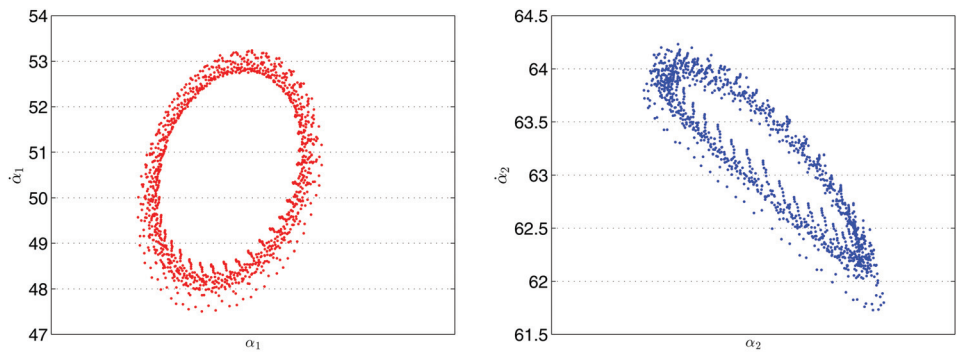

(*a*) (*b*)

Fig. 6 (*a*) The poincaré map for Initial$_1$ of the upstream set and (*b*) the poincaré map for Initial$_1$ of the downstream set

It is also of a great interest to present the transition from chaos to hyperchaos, in particular for an interconnected system. Figures 9, 10(*a*), and 10(*b*) reveal such a transition. Figure 9 shows a broad spectrum of Lyapunov exponents versus the equivalent b_{eqi}'s and μ_i's (as discussed in Sec. 3), which explicitly separates the chaotic and hyperchaotic domains. The chaotic domain, for the range of $2 \times 10^{-4} \leq b_{di} = \mu_i \leq 10^{-3}$ by presenting one positive Lyapunov exponent, is transmitted to the hyperchaotic one for the range of $10^{-7} \leq b_{di} = \mu_i < 2 \times 10^{-4}$, which presents two positive Lyapunov exponents. As discussed earlier, the attraction domain of a hyperchaotic response is relatively larger than that of the chaotic one, as can be observed in Figs. 10(*a*) and 10(*b*). Figures 10(*a*) and 10(*b*) present bifurcation diagrams versus the equivalent b_{eqi}'s and μ_i's for the upstream and downstream valves, respectively. The larger domains of attractions of the hyperchaotic responses, for both the valves, are distinguishable with respect to the chaotic ones. The hyperchaotic and chaotic domains of the downstream set are expectedly larger than those of the upstream set.

One of the crucial issues which needs to be investigated is the effects of dangerous behavior of a valve–actuator set on another one. Figures 11(*a*) and 11(*b*) present this interesting situation in which the upstream set is assumed to be chaotic by exposing to the critical values of $b_{d1} = \mu_1 = 10^{-7}$, and the downstream set is operated safely using $b_{d2} = \mu_2 = 10^{-1}$, for the second set of initial condition.

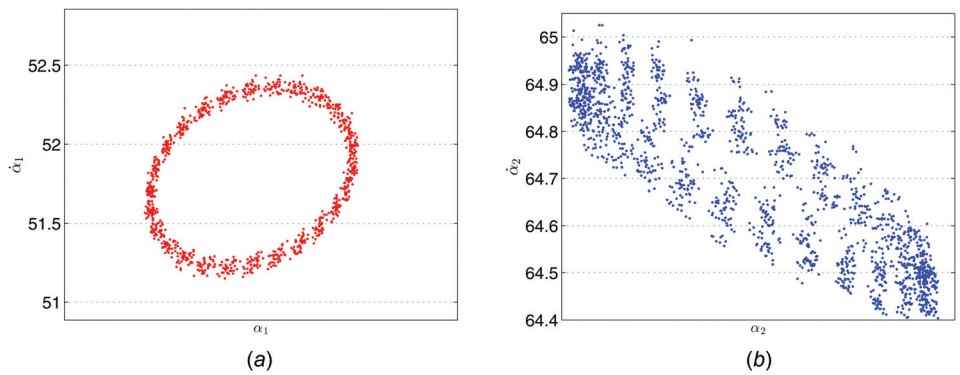

(*a*) (*b*)

Fig. 7 (*a*) The Poincaré map for Initial$_2$ of the upstream set and (*b*) the Poincaré map for Initial$_2$ of the downstream set

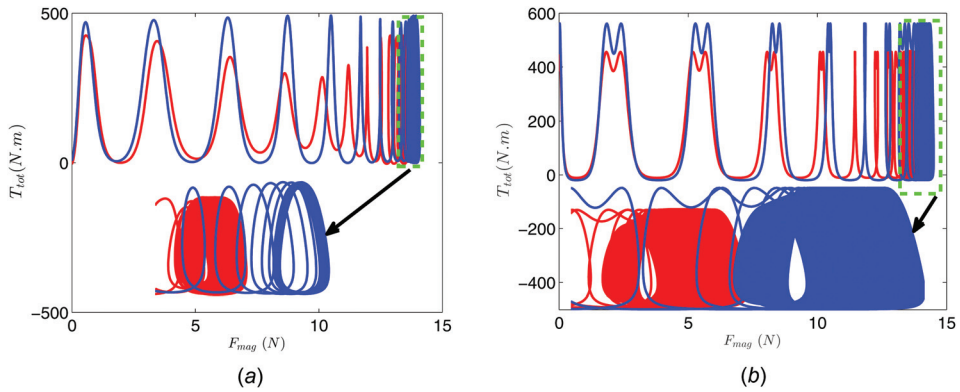

Fig. 8 (*a*) The sum of flow loads versus magnetic force of both the upstream and downstream sets for Initial$_1$ and (*b*) the sum of flow loads versus magnetic force of both the upstream and downstream sets for Initial$_2$

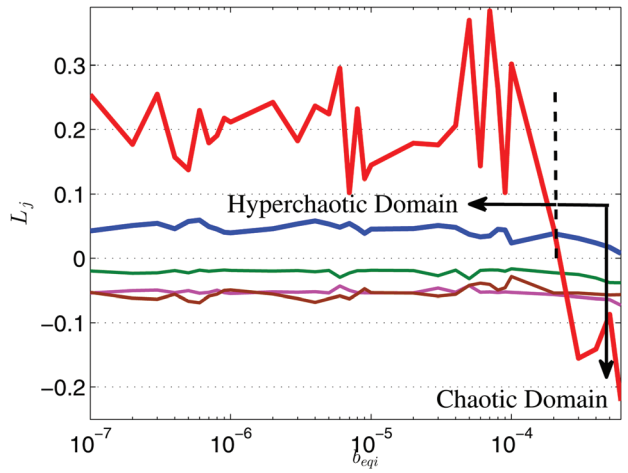

Fig. 9 A broad spectrum of Lyapunov exponents versus the equivalent b_{eqi}'s and μ_i's revealing transition from chaos to hyperchaos

The hyperchaotic motion of the upstream valve is again expected to be observed, but another smaller chaotic attractor, with a positive Lyapunov exponent of $L_1 = +0.013$, surprisingly emerges (Fig. 11(*a*)) which is significantly different from the previous case of Fig. 4(*b*). Its Poincaré map shown in Fig. 12(*a*) confirms the chaotic dynamics of the upstream set containing irregular points but expectedly different from the map presented in Fig. 7(*a*). It is of great interest to observe a very weak chaotic motion of the downstream valve as shown in Fig. 11(*b*), whereas a stable response was logically expected to be seen. Figure 12(*b*) is the Poincaré map of the downstream set revealing irregular points but too close to its equilibrium point. It is fairly straightforward to conclude that the chaotic motion of the upstream set is transmitted to the downstream one through the media trapped between them and subsequently affects its dynamics. Increasing the chaotic attractor domain of a set would accordingly magnify the domains of neighbor ones which would gradually cause failure of the whole network of thousands of valves–actuators. Such failures have to be avoided to reduce the considerable cost needed to restore the flow line.

5 Conclusions

This paper represented an interconnected nonlinear model of two actuators and valves subject to the sudden contraction. These dependencies among different components were formalized to yield a sixth-order dynamic model of the whole system. We established a stability map to yield a clear picture of stability/instability of the coupled network for some critical values of the equivalent viscous damping and the friction coefficient of the bearing area.

The coupled chaotic and hyperchaotic dynamics were captured and discussed. Some powerful tools of the nonlinear dynamic

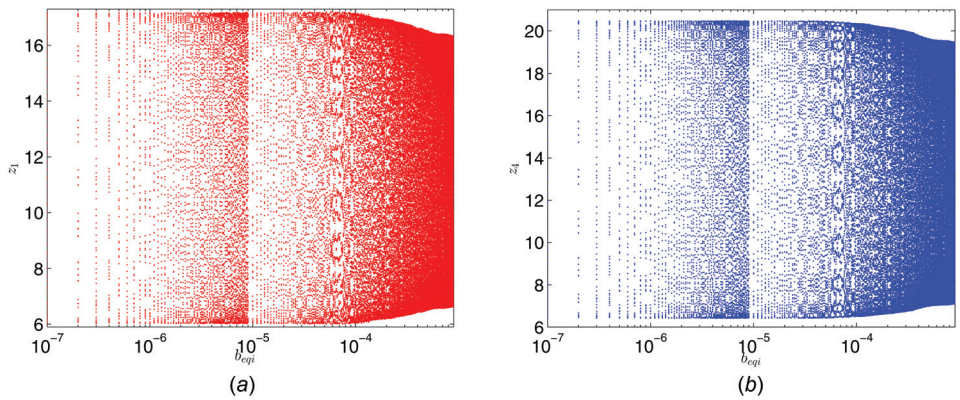

Fig. 10 (*a*) The bifurcation diagram versus the equivalent b_{eqi}'s and μ_i's for the upstream valve revealing transition from chaos to hyperchaos and (*b*) the bifurcation diagram versus the equivalent b_{eqi}'s and μ_i's for the downstream valve revealing transition from chaos to hyperchaos

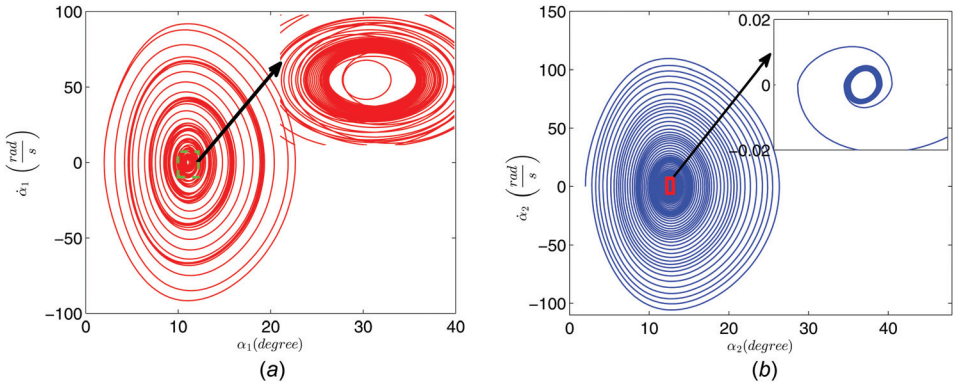

Fig. 11 (*a*) The phase portrait of the upstream set for Initial$_2$ and (*b*) the phase portrait of the downstream set for Initial$_2$

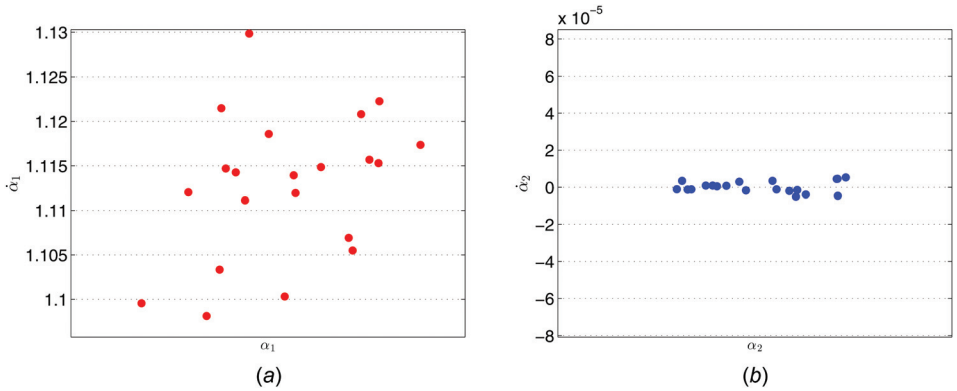

Fig. 12 (*a*) The poincaré map of the upstream set for Initial$_2$ and (*b*) the poincaré map of the downstream set for Initial$_2$

analysis were then employed, including Lyapunov exponents and Poincaré map, to characterize the responses obtained. We presented the expected larger hyperchaotic attractor domains in comparison with the chaotic ones. One and two positive Lyapunov exponents were shown to confirm the chaotic and hyperchaotic dynamics of the coupled actuated valves, respectively. The irregular Poincaré maps were also presented to support both the chaotic and hyperchaotic dynamics along with the positive Lyapunov exponents.

The upstream valve–actuator set was intentionally operated with the same initial condition and critical values of the hyperchaotic dynamics to evaluate its effects on a stable downstream set. The dynamics of the upstream set was surprisingly different by revealing a chaotic attractor demonstrated by its Poincaré map and a positive Lyapunov exponent. The downstream set was also affected by the chaotic dynamics of the upstream one by showing the irregular Poincaré map but too close to its equilibrium point.

We are currently focusing our efforts on developing a comprehensive model for *n* valves and actuators to be operated optimally and safely in series.

Acknowledgment

The experimental work of this research was supported by the Office of Naval Research Grant No. N00014/2008/1/0435. We appreciate this grant and the advice and direction provided by Mr. Anthony Seman III, the program manager.

References

[1] Naseradinmousavi, P., and Nataraj, C., 2011, "Nonlinear Mathematical Modeling of Butterfly Valves Driven by Solenoid Actuators," J. Appl. Math. Modell., **35**(5), pp. 2324–2335.

[2] Naseradinmousavi, P., and Nataraj, C., 2011, "A Chaotic Blue Sky Catastrophe of Butterfly Valves Driven by Solenoid Actuators," ASME Paper No. IMECE2011-62608.

[3] Naseradinmousavi, P., and Nataraj, C., 2012, "Transient Chaos and Crisis Phenomena in Butterfly Valves Driven by Solenoid Actuators," Commun. Nonlinear Sci. Numer. Simul., **17**(11), pp. 4336–4345.

[4] Naseradinmousavi, P., and Nataraj, C., 2013, "Optimal Design of Solenoid Actuators Driving Butterfly Valves," ASME J. Mech. Des., **135**(9), p. 094501.

[5] Naseradinmousavi, P., 2015, "A Novel Nonlinear Modeling and Dynamic Analysis of Solenoid Actuated Butterfly Valves Coupled in Series," ASME J. Dyn. Syst., Meas., Control, **137**(1), p. 014505.

[6] Naseradinmousavi, P., and Nataraj, C., 2015, "Design Optimization of Solenoid Actuated Butterfly Valves Dynamically Coupled in Series," ASME Paper No. DSCC2015-9605.

[7] Naseradinmousavi, P., 2015, "Optimal Design of Solenoid Actuated Butterfly Valves Dynamically Coupled in Series," ASME Paper No. IMECE2015-50094.

[8] Naseradinmousavi, P., Krstic, M., and Nataraj, C., 2016, "Design Optimization of Dynamically Coupled Actuated Butterfly Valves Subject to a Sudden Contraction," ASME J. Mech. Des., **138**(4), p. 041402.

[9] Sun, K., Liu, X., Zhu, C., and Sprott, J. C., 2012, "Hyperchaos and Hyperchaos Control of the Sinusoidally Forced Simplified Lorenz System," Nonlinear Dyn., **69**(3), pp. 1383–1391.

[10] Banerjee, T., Biswas, D., and Sarkar, B. C., 2013, "Anticipatory, Complete and Lag Synchronization of Chaos and Hyperchaos in a Nonlinear Delay-Coupled Time-Delayed System," Nonlinear Dyn., **72**(1), pp. 321–332.

[11] Boivin, N., Pierre, C., and Shaw, S. W., 1995, "Non-Linear Normal Modes, Invariance, and Modal Dynamics Approximations of Non-Linear Systems," J. Nonlinear Dyn., **8**(3), pp. 315–346.

[12] Belato, D., Weber, H. I., Balthazar, J. M., and Mook, D. T., 2001, "Chaotic Vibrations of a Nonideal Electro-Mechanical System," Int. J. Solids Struct., **38**(10–13), pp. 1699–1706.

[13] Ge, Z. M., and Lin, T. N., 2003, "Chaos, Chaos Control and Synchronization of Electro-Mechanical Gyrostat System," J. Sound Vib., **259**(3), pp. 585–603.

[14] Xie, W. C., Lee, H. P., and Lim, S. P., 2003, "Nonlinear Dynamic Analysis of MEMS Switches by Nonlinear Modal Analysis," J. Nonlinear Dyn., **31**(3), pp. 243–256.

[15] Wang, X.-Y., and Song, J.-M., 2009, "Synchronization of the Fractional Order Hyperchaos Lorenz Systems With Activation Feedback Control," Commun. Nonlinear Sci. Numer. Simul., **14**(8), pp. 3351–3357.

[16] Quan Dou, F., An Sun, J., Shan Duan, W., and Pu Lu, K., 2009, "Controlling Hyperchaos in the New Hyperchaotic System," Commun. Nonlinear Sci. Numer. Simul., **14**(2), pp. 552–559.
[17] Wu, W., and Chen, Z., 2010, "HOPF Bifurcation and Intermittent Transition to Hyperchaos in a Novel Strong Four-Dimensional Hyperchaotic System," Nonlinear Dyn., **60**(4), pp. 615–630.
[18] Choudhury, S. R., and Gorder, R. A. V., 2012, "Competitive Modes as Reliable Predictors of Chaos Versus Hyperchaos and as Geometric Mappings Accurately Delimiting Attractors," Nonlinear Dyn., **69**(4), pp. 2255–2267.
[19] Nik, H. S., and Gorder, R. A. V., 2013, "Competitive Modes for the Baier-Sahle Hyperchaotic Flow in Arbitrary Dimensions," Nonliear Dyn., **74**(3), pp. 581–590.
[20] Effati, S., Nik, H. S., and Jajarmi, A., 2013, "Hyperchaos Control of the Hyperchaotic Chen System by Optimal Control Design," Nonlinear Dyn., **73**(1), pp. 499–508.
[21] Munteanu, L., Brisan, C., Chiroiu, V., Dumitriu, D., and Ioan, R., 2014, "Chaoshyperchaos Transition in a Class of Models Governed by Sommerfeld Effect," Nonlinear Dyn., **78**(3), pp. 1877–1889.
[22] Kengne, J., Chedjou, J. C., Fozin, T. F., Kyamakya, K., and Kenne, G., 2014, "On the Analysis of Semiconductor Diode-Based Chaotic and Hyperchaotic Generators—A Case Study," Nonlinear Dyn., **77**(1), pp. 373–386.
[23] Zhou, P., and Yang, F., 2014, "Hyperchaos, Chaos, and Horseshoe in a 4D Nonlinear System With an Infinite Number of Equilibrium Points," Nonlinear Dyn., **76**(1), pp. 473–480.
[24] Liu, L., Ding, W., Liu, C., Ji, H., and Cao, C., 2014, "Hyperchaos Synchronization of Fractional-Order Arbitrary Dimensional Dynamical Systems Via Modified Sliding Mode Control," Nonlinear Dyn., **76**(4), pp. 2059–2071.
[25] Li, Q., Tang, S., Zeng, H., and Zhou, T., 2014, "On Hyperchaos in a Small Memristive Neural Network," Nonlinear Dyn., **78**(2), pp. 1087–1099.
[26] Lia, Q., Tanga, S., and Yang, X.-S., 2014, "Hyperchaotic Set in Continuous Chaos-Hyperchaos Transition," Commun. Nonlinear Sci. Numer. Simul., **19**(10), pp. 3718–3734.
[27] Park, J. Y., and Chung, M. K., 2006, "Study on Hydrodynamic Torque of a Butterfly Valve," ASME J. Fluids Eng., **128**(1), pp. 190–195.
[28] Leutwyler, Z., and Dalton, C., 2008, "A CFD Study of the Flow Field, Resultant Force, and Aerodynamic Torque on a Symmetric Disk Butterfly Valve in a Compressible Fluid," ASME J. Pressure Vessel Technol., **130**(2), pp. 139–147.
[29] Naseradinmousavi, P., 2012, "Nonlinear Modeling, Dynamic Analysis, and Optimal Design and Operation of Electromechanical Valve Systems," Ph.D. thesis, Villanova University, Villanova, PA.
[30] Bennett, C. O., and Myers, J. E., 1962, *Momentum, Heat, and Mass Transfer*, McGraw-Hill, New York.
[31] Massey, B. S., and Ward-Smith, J., 1998, *Mechanics of Fluids*, 7th ed., Taylor & Francis, London.
[32] AWWA, 2012, *Butterfly Valves: Torque, Head Loss, and Cavitation Analysis*, 2nd ed., American Water Works Association, Denver, CO.
[33] Nayfeh, A. H., and Balachandran, B., 1995, *Applied Nonlinear Dynamics: Analytical, Computational, and Experimental Methods*, Wiley-VCH Verlag GmbH, Weinheim, Germany.